UNIVERSIDAD DE CONCEPCIÓN

Centro de Investigación en Ingeniería Matemática (CI^{2}MA)

An a posteriori error estimator for a LPS method for Navier-Stokes equations

Rodolfo Araya, Ramiro Rebolledo

PREPRINT 2018-01

SERIE DE PRE-PUBLICACIONES

An a posteriori error estimator for a LPS method for Navier–Stokes equations

Rodolfo Araya[a], Ramiro Rebolledo[b]

[a]*Departamento de Ingeniería Matemática and CI²MA, Universidad de Concepción, Casilla 160-C, Concepción, Chile*
[b]*Departamento de Ingeniería Matemática, Universidad de Concepción, Casilla 160-C, Concepción, Chile*

Abstract

In this work we develop an a posteriori error estimator, of the hierarchical type, for the Local Projection Stabilized (LPS) finite element method introduced in [5], applied to the incompressible Navier–Stokes equations. The technique use the solution of locals problems posed on appropriate finite dimensional spaces of bubble-like functions, to approach the error. Several numerical tests confirm the theoretical properties of the estimator and its performance.

Keywords: Navier–Stokes equation, stabilized finite element scheme, a posteriori error estimates
2010 MSC: 65N12, 65N30

1. Introduction

The simulations of realistic fluid flows may be carried out by the Navier–Stokes equations, but it is not an easy task to compute accurate solutions to this equation, mainly because we need to capture small flow structures, which normally is prohibitively expensive if we use uniform refined meshes. Thus, numerical schemes ought to involve local mesh refinements which in turn demand prior knowledge on approximation errors. This adaptive strategy is behind the design of a posteriori error estimators, which have been developed for Navier–Stokes, applying mainly a residual strategy, i.e. computations of the norm of volumetric and edge residuals and not in solving local differential equations, (see, for instance [4], [11] and [21] and the references therein).

Another type of error estimators, called hierarchical estimators, were first introduced by Bank and collaborators in [7] and [6]. The idea here is to enrich the standard finite element subspace with some "bubble" like functions to improve the quality of the error estimator. This idea, which in practice is more expensive to compute than the residual, normally yields some better approximation of the true approximation error, with a better effectivity index. This hierarchical approach was extended in [2] to the advection-diffusion-reaction equation, in [1] to the generalized Stokes equations and later to the 2D steady incompressible Navier–Stokes equations, using a SUPG scheme, in [3].

On the other hand, in this work we mixed a stabilized scheme introduced in [5] with a hierarchical a posteriori error estimator, with the end of improve the quality of the numerical solution with a small computational effort. Stabilized schemes for fluid equations have a long history since the first works of Hughes, Brooks and Franca ([14], [20] or [17]). The main idea behind these methods is to add "stability" to the numerical solution of the problems, in particular overcoming the need that the discrete subspaces satisfy the Babuska–Brezzi condition, allowing, for instance, equal order of polynomials both for velocity and pressure, which is a very appreciated property at the moment of the numerical implementation. On the other hand,

Email addresses: rodolfo.araya@udec.cl (Rodolfo Araya), rrebolledo@ing-mat.udec.cl (Ramiro Rebolledo)

stabilized methods also help to diminish non physical instabilities coming from inner or boundary layers present, for example, when the advection is dominant with respect to viscosity.

In the present work, we extend the approach given in [3], to the Local Projection Stabilized (LPS) scheme introduced in [5] for the Navier–Stokes equations both in 2D as in 3D. This kind of stabilized methods, as most of stabilized ones, allow the use of equal order interpolation spaces, for velocity and pressure, which are easy to use in practice but that are no inf-sup stable. Besides that, the local projection methods, introduced originally in [10] for Stokes and in [12] for Oseen, are easier to compute than the residual based stabilized methods, avoiding the local computation of strong differential operators, decoupling the velocity and pressure terms in the stabilized terms, and have better approximation capabilities near the boundary.

Unfortunately, the LPS method is not strongly consistent, which is a major drawback when we try to develop an a posteriori error estimator, which is particularly difficult when we use low-order finite element spaces. Nevertheless, with our hierarchical approach we were able to overcome the lack of consistency, at the price of adding a higher order term to the reliability estimate. We have to mention that the consistency problem does not allow to use the standard techniques (see Verfürth in [30]) to develop an a posteriori error estimate based in the computations of the norm of the residuals terms, due to the difficulty to obtain volumetric and edge residuals in the reliability proof.

The outline of this work is as follows: in Section 2 we introduce our model problem and some useful preliminary results. In Section 3 we present the LPS method and its main approximation results. In Section 4 we define our a posteriori error estimator, of hierarchical type, and prove the equivalence of this error estimator with the approximation error, using an intermediate auxiliary problem. Finally, in Section 5, we present some numerical tests which allow us to assess the convergence property of the LPS method and the quality of our a posteriori error estimator.

2. Model problem and preliminary results

Let $\Omega \subset \mathbb{R}^d$ ($d = 2$ or $d = 3$) be a bounded polygonal open domain. The steady incompressible Navier–Stokes problem consists in finding a velocity vector field $\boldsymbol{u}$ and a pressure scalar field p such as

$$(\text{NS}) \begin{cases} -\nu\Delta\boldsymbol{u} + (\nabla\boldsymbol{u})\boldsymbol{u} + \nabla p &= \boldsymbol{f} \quad \text{in } \Omega, \\ \nabla\cdot\boldsymbol{u} &= 0 \quad \text{in } \Omega, \\ \boldsymbol{u} &= \boldsymbol{0} \quad \text{on } \partial\Omega, \end{cases}$$

where the fluid viscosity $\nu > 0$ and the force field $\boldsymbol{f} \in L^2(\Omega)^d$ are given. As usual, $L^2(\Omega)$ denotes the space of square integrable functions over Ω.

We utilize standard simplified terminology for Sobolev space, inner product and norms (see, e.g. [16]). In particular, if $\mathcal{O} \subseteq \Omega$, then $(\cdot,\cdot)_{\mathcal{O}}$ denotes the $L^2(\mathcal{O})$ inner product for scalar, vector or tensor valued functions, as appropriate. Also we denote by $\|\cdot\|_{m,\mathcal{O}}$ the usual norm of the Sobolev $H^m(\mathcal{O})$, with $m \geq 0$, and $H^{-1}(\mathcal{O})$ the dual space of $H_0^1(\mathcal{O})$ equipped with the dual norm $\|\cdot\|_{-1,\mathcal{O}}$.

Furthermore, we introduce the spaces

$$\mathbf{H} := H_0^1(\Omega)^d := \{\boldsymbol{v} \in H^1(\Omega)^d : \boldsymbol{v} = \boldsymbol{0} \text{ on } \partial\Omega\}$$

and

$$Q := L_0^2(\Omega) := \{q \in L^2(\Omega) : \int_\Omega q = 0\},$$

equipped with the norms $|\cdot|_{1,\Omega}$ and $\|\cdot\|_{0,\Omega}$, respectively, recalling that, thanks to Poincaré's inequality, the seminorm $|\cdot|_{1,\Omega}$ is indeed a norm on $\mathbf{H}$.

The standard weak formulation for the problem (NS) is the following: *Find* $(\boldsymbol{u}, p) \in \mathbf{H} \times Q$ *such that*

$$a(\boldsymbol{u}, \boldsymbol{v}) - b(\boldsymbol{u}, q) + b(\boldsymbol{v}, p) + c(\boldsymbol{u}; \boldsymbol{u}, \boldsymbol{v}) = (\boldsymbol{f}, \boldsymbol{v})_\Omega \tag{1}$$

for all $(\boldsymbol{v}, q) \in \mathbf{H} \times Q$, where the bilinear forms $a(\cdot, \cdot)$ and $b(\cdot, \cdot)$, and the trilinear form $c(\cdot\ ;\ \cdot, \cdot)$ are given by

$$a(\boldsymbol{u}, \boldsymbol{v}) := \nu\,(\nabla \boldsymbol{u}, \nabla \boldsymbol{v})_\Omega \qquad \forall \boldsymbol{u}, \boldsymbol{v} \in \mathbf{H}, \tag{2}$$

$$b(\boldsymbol{v}, q) := -(q, \nabla \cdot \boldsymbol{v})_\Omega \qquad \forall q \in Q, \forall \boldsymbol{v} \in \mathbf{H}, \tag{3}$$

$$c(\boldsymbol{u}; \boldsymbol{v}, \boldsymbol{w}) := ((\nabla \boldsymbol{v})\boldsymbol{u}, \boldsymbol{w})_\Omega \qquad \forall \boldsymbol{u}, \boldsymbol{v}, \boldsymbol{w} \in \mathbf{H}. \tag{4}$$

In addition, we introduce the symmetric bilinear form $d : Q \times Q \to \mathbb{R}$ given by

$$d(p, q) := \frac{1}{\nu}\,(p, q)_\Omega.$$

The bilinear forms $a(\cdot, \cdot)$ and $d(\cdot, \cdot)$ induce the norms

$$\|\boldsymbol{v}\|_a := a(\boldsymbol{v}, \boldsymbol{v})^{1/2} \quad \forall \boldsymbol{v} \in \mathbf{H},$$
$$\|q\|_d := d(q, q)^{1/2} \quad \forall q \in Q.$$

Also, we denote by $\|\cdot\|_{a,\mathcal{O}}$ the norm induced by $a(\cdot, \cdot)$ on the set $\mathcal{O} \subset \Omega$. We equip the space $\mathbf{H} \times Q$ with the product norm given by

$$\|(\boldsymbol{v}, q)\| := \left\{ \|\boldsymbol{v}\|_a^2 + \|q\|_d^2 \right\}^{1/2} \quad \forall (\boldsymbol{v}, q) \in \mathbf{H} \times Q.$$

The next result states some important inequalities related to the forms a, b and c.

Lemma 2.1. *Let $a(\cdot, \cdot)$ and $b(\cdot, \cdot)$ be the bilinear forms given by* (2) *and* (3)*, respectively, and let $c(\cdot\ ;\ \cdot, \cdot)$ be the trilinear form given by* (4)*. Then*

$$|a(\boldsymbol{v}, \boldsymbol{w})| \le \|\boldsymbol{v}\|_a \|\boldsymbol{w}\|_a \qquad \forall \boldsymbol{v}, \boldsymbol{w} \in \mathbf{H},$$

$$|b(\boldsymbol{v}, q)| \le \sqrt{d}\,\|\boldsymbol{v}\|_a \|q\|_d \qquad \forall (\boldsymbol{v}, q) \in \mathbf{H} \times Q,$$

$$\sup_{\substack{\boldsymbol{v} \in \mathbf{H} \\ \boldsymbol{v} \neq \boldsymbol{0}}} \frac{b(\boldsymbol{v}, q)}{\|\boldsymbol{v}\|_a} \ge \alpha_b \|q\|_d \qquad \forall q \in Q,$$

$$c(\boldsymbol{w}; \boldsymbol{u}, \boldsymbol{v}) \le \beta\,|\boldsymbol{w}|_{1,\Omega} |\boldsymbol{u}|_{1,\Omega} |\boldsymbol{v}|_{1,\Omega} \qquad \forall \boldsymbol{u}, \boldsymbol{v}, \boldsymbol{w} \in \mathbf{H},$$

where α_b and β are positive constants depending only on Ω. Moreover, for all $\boldsymbol{u}, \boldsymbol{v}, \boldsymbol{w} \in H^1(\Omega)^d$ such that $\nabla \cdot \boldsymbol{w} = 0$ and $\boldsymbol{w} \cdot \boldsymbol{n} = 0$, it holds

$$c(\boldsymbol{w}; \boldsymbol{u}, \boldsymbol{v}) = -c(\boldsymbol{w}; \boldsymbol{v}, \boldsymbol{u}),$$
$$c(\boldsymbol{w}; \boldsymbol{v}, \boldsymbol{v}) = 0.$$

Proof. The first two statements are straightforward and the others are classical results (see, for instance, [19]).

The well-posedness of the variational problem (1) is ensured by the following result

Theorem 2.1. *Assume that ν and $\boldsymbol{f} \in L^2(\Omega)^d$ satisfy the following condition:*

$$|(\boldsymbol{f}, \boldsymbol{v})_\Omega| \le \gamma \frac{\nu^2}{\beta}\,|\boldsymbol{v}|_{1,\Omega} \quad \forall \boldsymbol{v} \in \mathbf{H} \tag{5}$$

for some fixed number $\gamma \in [0, 1[$. Then, there exists a unique solution $(\boldsymbol{u}, p) \in \mathbf{H} \times Q$ of (1) *and it holds*

$$|\boldsymbol{u}|_{1,\Omega} \le \gamma \frac{\nu}{\beta}.$$

PROOF. See Theorem 2.4, Chapter IV in [19].

In order to introduce finite element subspaces, let $\{\mathcal{T}_h\}_{h>0}$ be a regular family of triangulations of $\bar{\Omega}$ composed by elements K (triangles or tetrahedra in 2D or 3D, respectively) of diameter h_K such that $\bar{\Omega} = \cup\{K : K \in \mathcal{T}_h\}$ and define $h := \max\{h_K : K \in \mathcal{T}_h\}$. The finite element subspaces to be used in this work are defined as follows

$$\mathbf{H}_h := \{\boldsymbol{v} \in \mathcal{C}^0(\bar{\Omega})^d : \ \boldsymbol{v}|_K \in \mathbb{P}_1(K)^d, \ \forall K \in \mathcal{T}_h\} \cap \mathbf{H},$$

and

$$Q_h := \{q \in L^2(\Omega) : \ q|_K \in \mathbb{P}_0(K), \ \forall K \in \mathcal{T}_h\} \cap Q,$$

where $\mathbb{P}_l(K)$ denotes the space of polynomials of total degree less than or equal to l, with $l = 0, 1$. In turn, we denote by $\mathcal{E}_\Omega$ the set of all the interior edges ($d = 2$) or faces ($d = 3$) of $\mathcal{T}_h$ and h_F the diameter of each $F \in \mathcal{E}_\Omega$.

In the sequel we will denote by C a generic positive constant, independent of the discretization parameter h and the viscosity ν, which may take different values at different places.

Given $K \in \mathcal{T}_h$ and $F \in \mathcal{E}_\Omega$ we define the following neighborhoods:

$$\omega_K := \bigcup_{\mathcal{E}(K)\cap\mathcal{E}(K')\neq\emptyset} K', \qquad \widetilde{\omega}_K := \bigcup_{\mathcal{N}(K)\cap\mathcal{N}(K')\neq\emptyset} K',$$

$$\omega_F := \bigcup_{F\in\mathcal{E}(K')} K', \qquad \widetilde{\omega}_F := \bigcup_{\mathcal{N}(F)\cap\mathcal{N}(K')\neq\emptyset} K',$$

where $\mathcal{E}(K)$ denotes the set of edges (or faces if $d = 3$) of the element K, $\mathcal{N}(K)$ the set of nodes of K and $\mathcal{N}(F)$ the set of nodes of F.

Let $\mathcal{I}_h : \mathbf{H} \longrightarrow \mathbf{H}_h$ be the Clément interpolation operator introduced in [15]. It can be easily shown (see [15, 16] for details) that the Clément interpolation operator satisfies the following estimates

$$\|\boldsymbol{v} - \mathcal{I}_h\boldsymbol{v}\|_{0,K} \leq C\,\nu^{-1/2} h_K \,\|\boldsymbol{v}\|_{a,\widetilde{\omega}_K}, \tag{6}$$

$$\|\boldsymbol{v} - \mathcal{I}_h\boldsymbol{v}\|_{0,F} \leq C\,\nu^{-1/2} h_F^{1/2} \,\|\boldsymbol{v}\|_{a,\widetilde{\omega}_F}, \tag{7}$$

$$\|\mathcal{I}_h\boldsymbol{v}\|_{a,K} \leq C\,\|\boldsymbol{v}\|_{a,\widetilde{\omega}_K}, \tag{8}$$

for all $\boldsymbol{v} \in H^1(\Omega)^d$.

Finally, for each $K \in \mathcal{T}_h$, we denote by $\Pi_K q$ the average of a function $q \in L^2(K)$, i.e.,

$$\Pi_K q := \frac{1}{|K|}\int_K q \,\mathrm{d}x.$$

Lemma 2.2.

$$\|v - \Pi_K v\|_{0,K} \leq \frac{h_K}{\pi}|v|_{1,K} \qquad \forall v \in H^1(K), \tag{9}$$

$$\|\Pi_K v\|_{0,K} \leq \|v\|_{0,K} \qquad \forall v \in L^2(K). \tag{10}$$

PROOF. See Proposition 1.134 and Lemma 1.131 in [16].

Hereafter, we will use intensively the *fluctuation* operator χ_h defined by $\chi_h := \mathbf{I} - \Pi_K$, where $\mathbf{I}$ is the identity operator. Observe that, from Lemma 2.2, it holds

$$\|\chi_h(\boldsymbol{x}\cdot\Pi_K\boldsymbol{v})\|_{0,K} \leq \frac{h_K}{\pi}\|\boldsymbol{v}\|_{0,K} \qquad \forall \boldsymbol{v} \in L^2(K)^d. \tag{11}$$

Finally, we define the jump of a function q across $F \in \mathcal{E}_h$ by

$$[\![q]\!]_F(\boldsymbol{x}) := \lim_{\delta\to 0^+} q(\boldsymbol{x} + \delta\boldsymbol{n}_F) - \lim_{\delta\to 0^+} q(\boldsymbol{x} - \delta\boldsymbol{n}_F)$$

where $\boldsymbol{n}_F$ is the outward normal vector at F with respect to an element K of $\mathcal{T}_h$.

3. The local projection stabilized method

The Local Projection Stabilized (LPS) method for the Navier–Stokes equations, introduced and analyzed in [5], has the following form: *Find* $(\boldsymbol{u}_h, p_h) \in \mathbf{H}_h \times Q_h$ *such that*

$$
(\text{LPS}) \begin{cases} \nu\,(\nabla \boldsymbol{u}_h, \nabla \boldsymbol{v}_h)_\Omega + ((\nabla \boldsymbol{u}_h)\boldsymbol{u}_h, \boldsymbol{v}_h)_\Omega - (p_h, \nabla\cdot \boldsymbol{v}_h)_\Omega + (q_h, \nabla\cdot \boldsymbol{u}_h)_\Omega \\ + \sum_{K\in\mathcal{T}_h} \dfrac{\alpha_K}{\nu}(\chi_h(\boldsymbol{x}\cdot \Pi_K[(\nabla \boldsymbol{u}_h)\boldsymbol{u}_h]), \chi_h(\boldsymbol{x}\cdot \Pi_K[(\nabla \boldsymbol{v}_h)\boldsymbol{u}_h]))_K \\ + \sum_{K\in\mathcal{T}_h} \dfrac{\gamma_K}{\nu}(\chi_h(\boldsymbol{x}\nabla\cdot \boldsymbol{u}_h), \chi_h(\boldsymbol{x}\nabla\cdot \boldsymbol{v}_h))_K + \sum_{F\in\mathcal{E}_\Omega} \tau_F([\![p_h]\!], [\![q_h]\!])_F = (\boldsymbol{f}, \boldsymbol{v}_h)_\Omega, \end{cases}
$$

where the stabilization parameters are given by

$$
\alpha_K := \frac{1}{\max\{1, Pe_K\}} \quad \text{and} \quad \gamma_K := \frac{1}{\max\{1, \frac{Pe_K}{24}\}},
$$

with

$$
Pe_K := \frac{|\boldsymbol{u}_h|_K h_K}{18\,\nu} \quad \text{and} \quad |\boldsymbol{u}_h|_K := \frac{\|\boldsymbol{u}_h\|_{0,K}}{|K|^{\frac{1}{2}}},
$$

and

$$
\tau_F := \begin{cases} \dfrac{h_F}{12\,\nu}, \quad \text{if } |\boldsymbol{u}_h|_F = 0, \\ \dfrac{1}{2\,|\boldsymbol{u}_h|_F} - \dfrac{1}{|\boldsymbol{u}_h|_F\,(1-\exp(Pe_F))}\Big(1 + \dfrac{1}{Pe_F}(1-\exp(Pe_F))\Big), \quad \text{otherwise.} \end{cases}
$$

Here

$$
Pe_F := \frac{|\boldsymbol{u}_h|_F\, h_F}{\nu} \quad \text{with} \quad |\boldsymbol{u}_h|_F := \frac{\|\boldsymbol{u}_h\|_{0,F}}{h_F^{1/2}}.
$$

We recall, from Lemma 2 in [8], that τ_F satisfies

$$
\tau_F \le C\,\frac{h_F}{\nu}
$$

for all $F \in \mathcal{E}_\Omega$.

Remark 3.1. *Note that the method LPS has the disadvantage of being non consistent, which complicate the a priori and a posteriori analysis. On the other hand, LPS is easier to implement than the traditional residual projection methods (RELP). Finally, note that in the presence of Neumann boundary conditions, we only need to change the jump term accordingly.*

The well-posedness and error estimates for the LPS method were studied in [5], for completeness we present some of the main results concerning existence and uniqueness of the discrete solution, as well as error bounds.

Theorem 3.1. *There is a positive constant C, independent of h and ν, such that if*

$$
\frac{h^{1/2}}{\nu^2}\|\boldsymbol{f}\|_{-1,\Omega} \le C,
$$

then LPS problem admits at least one solution.

Proof. See Theorem 3.4 in [5].

Theorem 3.2. *There exists a positive constant C, independent of h and ν, such that if*

$$\frac{1}{\nu}\left\{1+\frac{1}{\nu^{3/2}}\right\}(1+h)^2 < C,$$

then the solution of the LPS problem is unique.

PROOF. See Theorem 3.5 in [5].

The next theorem establishes an optimal convergence result of the LPS method in the natural norm.

Theorem 3.3. *Assume that $(\boldsymbol{u},p)$ belongs to the space $H^2(\Omega)^d \times H^1(\Omega)$. Then there exists a positive constant h_0, such that for all h with $0<h\leq h_0$, the following estimate holds*

$$\left\{|\boldsymbol{u}-\boldsymbol{u}_h|^2_{1,\Omega}+\|p-p_h\|^2_{0,\Omega}\right\}^{1/2} \;\leq\; C\,h,$$

where $C>0$ does not depend on h but can depend on ν.

PROOF. See Theorem 4.4 in [5].

4. A Hierarchical Error Estimator

In this section we propose and analyze a hierarchical estimator for the LPS method adapting the ideas of [3] to our problem.

4.1. The Auxiliary Problem

In what follows, the functions $\boldsymbol{e}$ and E stand for the velocity and pressure approximation errors, i.e.,

$$\begin{aligned}\boldsymbol{e} &:= \boldsymbol{u}-\boldsymbol{u}_h,\\ E &:= p-p_h.\end{aligned}$$

In the sequel we will need the following linear auxiliary problem: *Find $(\boldsymbol{\phi},\psi)\in\mathbf{H}\times Q$ such that*

$$a(\boldsymbol{\phi},\boldsymbol{v})+d(\psi,q)=a(\boldsymbol{e},\boldsymbol{v})-b(\boldsymbol{e},q)+b(\boldsymbol{v},E)+l(\boldsymbol{u};\boldsymbol{u}_h,\boldsymbol{v}) \quad \forall(\boldsymbol{v},q)\in\mathbf{H}\times Q, \tag{12}$$

where

$$l(\boldsymbol{u};\boldsymbol{u}_h,\boldsymbol{v}) := c(\boldsymbol{u};\boldsymbol{u},\boldsymbol{v})-c(\boldsymbol{u}_h;\boldsymbol{u}_h,\boldsymbol{v}).$$

Clearly, the well-posedness of the above system arises from the ellipticity of $a(\cdot,\cdot)$ and $d(\cdot,\cdot)$ on $\mathbf{H}$ and Q, respectively.

Next, we establish an equivalence between the norms of $(\boldsymbol{e},E)\in\mathbf{H}\times Q$ and the norms of the solution $(\boldsymbol{\phi},\psi)\in\mathbf{H}\times Q$ of (12), thus opening the door to design an error estimate based on the functions $(\boldsymbol{\phi},\psi)$ only.

Theorem 4.1. *Assume that* (5) *holds and $|\boldsymbol{e}|_{1,\Omega}$ is sufficiently small in the sense that there exists $\varepsilon>0$ such that*

$$\gamma+\frac{\varepsilon^2}{2}+\frac{\beta}{\nu}|\boldsymbol{e}|_{1,\Omega}<1.$$

Then, there exists positive constants C_1 and C_2, independent of h, such that

$$C_1\left\{\|\boldsymbol{\phi}\|^2_a+\|\psi\|^2_d\right\}\leq\|\boldsymbol{e}\|^2_a+\|E\|^2_d\leq C_2\left\{\|\boldsymbol{\phi}\|^2_a+\|\psi\|^2_d\right\}.$$

PROOF. See Theorem 4.1 in [3].

From the definition of $\boldsymbol{e}$ and E, the auxiliary problem (12) is equivalent to

$$a(\boldsymbol{\phi},\boldsymbol{v})+d(\psi,q)=(\boldsymbol{f},\boldsymbol{v})_\Omega-a(\boldsymbol{u}_h,\boldsymbol{v})+b(\boldsymbol{u}_h,q)-b(\boldsymbol{v},p_h)-c(\boldsymbol{u}_h;\boldsymbol{u}_h,\boldsymbol{v}) \tag{13}$$

for all $(\boldsymbol{v},q)\in\mathbf{H}\times Q$. The above equation can be rewritten in a more compact form as

$$a(\boldsymbol{\phi},\boldsymbol{v})+d(\psi,q)=\mathcal{R}_h(\boldsymbol{v},q)\quad\forall(\boldsymbol{v},q)\in\mathbf{H}\times Q,$$

where $\mathcal{R}_h\in(\mathbf{H}\times Q)'$ stands for the residual functional given by

$$\mathcal{R}_h(\boldsymbol{v},q):=(\boldsymbol{f},\boldsymbol{v})_\Omega-a(\boldsymbol{u}_h,\boldsymbol{v})+b(\boldsymbol{u}_h,q)-b(\boldsymbol{v},p_h)-c(\boldsymbol{u}_h;\boldsymbol{u}_h,\boldsymbol{v})\quad\forall(\boldsymbol{v},q)\in\mathbf{H}\times Q.$$

Remark 4.1. *Note that the auxiliary problem* (12)*, or equivalently* (13)*, can be decoupled in two different problems. First, taking* $\boldsymbol{v}=\mathbf{0}$ *in* (13) *we obtain*

$$d(\psi,q)=b(\boldsymbol{u}_h,q)\quad\forall q\in Q,$$

now, using that $\nabla\cdot\boldsymbol{u}_h\in Q$*, we get that*

$$\psi=-\nu\,\nabla\cdot\boldsymbol{u}_h. \tag{14}$$

Second, taking $q=0$ *in* (13)*, we arrive at*

$$a(\boldsymbol{\phi},\boldsymbol{v})=\mathcal{R}_h^1(\boldsymbol{v})\qquad\forall\boldsymbol{v}\in\mathbf{H}, \tag{15}$$

where $\mathcal{R}_h^1\in\mathbf{H}'$ *is given by the expression*

$$\mathcal{R}_h^1(\boldsymbol{v}):=(\boldsymbol{f},\boldsymbol{v})_\Omega-a(\boldsymbol{u}_h,\boldsymbol{v})-b(\boldsymbol{v},p_h)-c(\boldsymbol{u}_h;\boldsymbol{u}_h,\boldsymbol{v})\qquad\forall\boldsymbol{v}\in\mathbf{H}.$$

An equivalent and useful expression for $\mathcal{R}_h^1$ is obtained using integration by parts, which leads to

$$\mathcal{R}_h^1(\boldsymbol{v})=\sum_{K\in\mathcal{T}_h}(\boldsymbol{R}_K,\boldsymbol{v})_K+\sum_{F\in\mathcal{E}_\Omega}(\boldsymbol{R}_F,\boldsymbol{v})_F,$$

where $\boldsymbol{R}_K$ and $\boldsymbol{R}_F$ are the local residuals defined by

$$\boldsymbol{R}_K:=(\boldsymbol{f}+\nu\,\Delta\boldsymbol{u}_h-(\nabla\boldsymbol{u}_h)\boldsymbol{u}_h-\nabla p_h)|_K\quad\text{ and }\quad\boldsymbol{R}_F:=[\![-\nu\,\partial_{\boldsymbol{n}}\boldsymbol{u}_h+p_h\boldsymbol{n}]\!]_F.$$

The following technical result will be useful in the sequel.

Lemma 4.1. *For all* $\boldsymbol{v}_h\in\mathbf{H}_h$ *it holds*

$$\mathcal{R}_h^1(\boldsymbol{v}_h)\le C\left[\sum_{K\in\mathcal{T}_h}\frac{h_K^4}{\nu^3}\Big\{\big(\|\boldsymbol{R}_K\|_{0,K}+\|\boldsymbol{f}\|_{0,K}\big)\|\boldsymbol{u}_h\|_{\infty,K}+\|\nabla\cdot\boldsymbol{u}_h\|_{0,K}\Big\}^2\right]^{1/2}\|\boldsymbol{v}_h\|_a.$$

Proof. From the definition of $\mathcal{R}_h^1$, using LPS scheme with $q_h=0$ and recalling that $\boldsymbol{u}_h|_K$ and $p_h|_K$ are a linear and constant polynomial in each $K\in\mathcal{T}_h$, respectively, it holds

$$\begin{aligned}
&\mathcal{R}_h^1(\boldsymbol{v}_h)=\ (\boldsymbol{f},\boldsymbol{v}_h)_\Omega-a(\boldsymbol{u}_h,\boldsymbol{v}_h)-b(\boldsymbol{v}_h,p_h)-c(\boldsymbol{u}_h;\boldsymbol{u}_h,\boldsymbol{v}_h)\\
&=\sum_{K\in\mathcal{T}_h}\Big\{\frac{\alpha_K}{\nu}(\chi_h(\boldsymbol{x}\cdot\Pi_K[(\nabla\boldsymbol{u}_h)\boldsymbol{u}_h]),\chi_h(\boldsymbol{x}\cdot\Pi_K[(\nabla\boldsymbol{v}_h)\boldsymbol{u}_h]))_K+\frac{\gamma_K}{\nu}(\chi_h(\boldsymbol{x}\nabla\cdot\boldsymbol{u}_h),\chi_h(\boldsymbol{x}\nabla\cdot\boldsymbol{v}_h))_K\Big\}\\
&=\sum_{K\in\mathcal{T}_h}\Big\{\frac{\alpha_K}{\nu}\Big[-(\chi_h(\boldsymbol{x}\cdot\Pi_K[\boldsymbol{R}_K]),\chi_h(\boldsymbol{x}\cdot\Pi_K[(\nabla\boldsymbol{v}_h)\boldsymbol{u}_h]))_K+(\chi_h(\boldsymbol{x}\cdot\Pi_K[\boldsymbol{f}]),\chi_h(\boldsymbol{x}\cdot\Pi_K[(\nabla\boldsymbol{v}_h)\boldsymbol{u}_h]))_K\Big]\\
&\qquad+\frac{\gamma_K}{\nu}(\chi_h(\boldsymbol{x}\nabla\cdot\boldsymbol{u}_h),\chi_h(\boldsymbol{x}\nabla\cdot\boldsymbol{v}_h))_K\Big\}.
\end{aligned}\tag{16}$$

Thus, using Hölder's inequality, (11), (16), Cauchy–Schwarz's inequality, and recalling that $\alpha_K, \gamma_K \leq 1$, we obtain

$$\begin{aligned}
\mathcal{R}_h^1(\boldsymbol{v}_h) &\leq C \sum_{K\in\mathcal{T}_h} \frac{h_K^2}{\nu}\Big\{\big(\|\boldsymbol{R}_K\|_{0,K} + \|\boldsymbol{f}\|_{0,K}\big)\|\boldsymbol{u}_h\|_{\infty,K}\|\nabla\boldsymbol{v}_h\|_{0,K} + \|\nabla\cdot\boldsymbol{u}_h\|_{0,K}\|\nabla\cdot\boldsymbol{v}_h\|_{0,K}\Big\} \\
&\leq C \sum_{K\in\mathcal{T}_h} \frac{h_K^2}{\nu}\Big\{\big(\|\boldsymbol{R}_K\|_{0,K} + \|\boldsymbol{f}\|_{0,K}\big)\|\boldsymbol{u}_h\|_{\infty,K} + \|\nabla\cdot\boldsymbol{u}_h\|_{0,K}\Big\}\|\nabla\boldsymbol{v}_h\|_{0,K} \\
&\leq C \left[\sum_{K\in\mathcal{T}_h} \frac{h_K^4}{\nu^3}\Big\{\big(\|\boldsymbol{R}_K\|_{0,K} + \|\boldsymbol{f}\|_{0,K}\big)\|\boldsymbol{u}_h\|_{\infty,K} + \|\nabla\cdot\boldsymbol{u}_h\|_{0,K}\Big\}^2\right]^{1/2} \|\boldsymbol{v}_h\|_a.
\end{aligned}$$

Remark 4.2. *The equivalence result in Theorem 4.1 can be rewritten using the characterization of ψ, given in* (14)*, as follows*

$$C_1\left\{\|\boldsymbol{\phi}\|_a^2 + \nu\,\|\nabla\cdot\boldsymbol{u}_h\|_{0,\Omega}^2\right\} \leq \|\boldsymbol{e}\|_a^2 + \|E\|_d^2 \leq C_2\left\{\|\boldsymbol{\phi}\|_a^2 + \nu\,\|\nabla\cdot\boldsymbol{u}_h\|_{0,\Omega}^2\right\}. \tag{17}$$

Therefore, we only need to estimate $\|\boldsymbol{\phi}\|_a$ using an a posteriori error estimator. This idea is pursued in the next section.

4.2. Hierarchical Error Estimator

Following closely the ideas of [1] and [3], let $\mathbf{W}_h$ be a finite element subspace such that $\mathbf{H}_h \subseteq \mathbf{W}_h \subseteq \mathbf{H}$. Let us suppose that $\mathbf{W}_h$ can be decomposed in the following way

$$\mathbf{W}_h = \mathbf{H}_h + \sum_{K\in\mathcal{T}_h} \mathbf{H}_K^b + \sum_{F\in\mathcal{E}_\Omega} \mathbf{H}_F^b,$$

where the finite dimensional subspaces $\mathbf{H}_K^b$ and $\mathbf{H}_F^b$ satisfy

$$\mathbf{H}_K^b \subset H_0^1(K)^d \quad \text{and} \quad \mathbf{H}_F^b \subset H_0^1(\omega_F)^d.$$

Associated to each subspace $\mathbf{H}_S^b$, with $S = K$ or F, there is a projection operator $P_S : \mathbf{H} \longrightarrow \mathbf{H}_S^b$ defined as the solution of the local problem

$$a(P_S\boldsymbol{v}, \boldsymbol{v}_S) = a(\boldsymbol{v}, \boldsymbol{v}_S) \quad \forall \boldsymbol{v}_S \in \mathbf{H}_S^b. \tag{18}$$

Thus we define our *a posteriori* error estimator η_H by

$$\eta_H := \left\{\sum_{K\in\mathcal{T}_h} a(P_K\boldsymbol{\phi}, P_K\boldsymbol{\phi}) + \sum_{F\in\mathcal{E}_\Omega} a(P_F\boldsymbol{\phi}, P_F\boldsymbol{\phi})\right\}^{1/2}. \tag{19}$$

Using the definition of $\boldsymbol{\phi}$ we obtain that $P_S\boldsymbol{\phi}$, with $S = K$ or F, is the solution of the local problem

$$a(P_S\boldsymbol{\phi}, \boldsymbol{v}_S) = \mathcal{R}_h^1(\boldsymbol{v}_S) \quad \forall \boldsymbol{v}_S \in \mathbf{H}_S^b. \tag{20}$$

Remark 4.3. *Notice that the solution $\boldsymbol{\phi}$ of* (15)*, used throughout previous estimates, does not need to be computed but only its projection $P_S\boldsymbol{\phi}$ onto finite dimensional subspaces $\mathbf{H}_S^b$.*

Remark 4.4. *The linear local problem* (20) *incorporates the Navier–Stokes non-linearity through its right hand side. This way of accounting for non-linearities in the a posteriori estimator represents a compromise between low computational cost and accuracy in the context of high speed flow.*

We also require that the local subspaces $\mathbf{H}^b_K$ and $\mathbf{H}^b_F$, hereafter called *bubble* subspaces, be piecewise affine-equivalent to a finite-dimensional space on a reference configuration, so that the following estimate holds:

$$\|\mathbf{b}_S\|^2_{0,K} \leq Ch_K^2\,|\mathbf{b}_S|^2_{1,K} \quad \forall \mathbf{b}_S \in \mathbf{H}^b_S,\ S = K \text{ or } F,$$

for all $K \in \mathcal{T}_h$.

Second, the bubble spaces must fulfil the following inf-sup conditions: there exists $\beta^* > 0$, independent of h and ν, such that

$$\sup_{\substack{\mathbf{b}_K \in \mathbf{H}^b_K \\ \mathbf{b}_K \neq \mathbf{0}}} \frac{(\mathbf{b}_K, \boldsymbol{R}_K)_K}{\|\mathbf{b}_K\|_{a,K}} \geq \beta^* \nu^{-1/2} h_K \|\boldsymbol{R}_K\|_{0,K} \quad \forall K \in \mathcal{T}_h, \tag{21}$$

$$\sup_{\substack{\mathbf{b}_F \in \mathbf{H}^b_F \\ \mathbf{b}_F \neq \mathbf{0}}} \frac{(\mathbf{b}_F, \boldsymbol{R}_F)_F}{\|\mathbf{b}_F\|_{a,\omega_F}} \geq \beta^* \nu^{-1/2} h_F^{1/2} \|\boldsymbol{R}_F\|_{0,F} \quad \forall F \in \mathcal{E}_\Omega. \tag{22}$$

In [1, Appendix B] was proved that the following pair of bubble subspaces satisfy conditions (21) and (22)

$$\begin{aligned} \mathbf{H}^b_K &= \langle \{ b_K\, \boldsymbol{R}_K \} \rangle \qquad \forall K \in \mathcal{T}_h, \\ \mathbf{H}^b_F &= \langle \{ b_F\, \boldsymbol{R}_F \} \rangle \qquad \forall F \in \mathcal{E}_\Omega, \end{aligned}$$

where b_K and b_F are the standard polynomial bubble functions defined with respect to the barycentric coordinates. We recall that $\mathbf{H}^b_F$ is well defined because in our case $\boldsymbol{R}_F$ is constant on each $F \in \mathcal{E}_\Omega$.

The next result is recalled as it is needed for the proof of the reliability of our estimator.

Lemma 4.2. *Suppose that* (21) *and* (22) *hold. Then,*

$$\begin{aligned} \mathcal{R}^1_h(\boldsymbol{v}) \leq & C\nu^{1/2} \Bigg\{ \sum_{K \in \mathcal{T}_h} h_K^{-1} a(P_K\boldsymbol{\phi}, P_K\boldsymbol{\phi})^{1/2} \|\boldsymbol{v}\|_{0,K} \\ & + \sum_{F \in \mathcal{E}_\Omega} h_F^{-1/2} \left[a(P_F\boldsymbol{\phi}, P_F\boldsymbol{\phi})^{1/2} + \sum_{K' \subset \omega_F} a(P_{K'}\boldsymbol{\phi}, P_{K'}\boldsymbol{\phi})^{1/2} \right] \|\boldsymbol{v}\|_{0,F} \Bigg\} \end{aligned}$$

for all $\boldsymbol{v}$ *in* $\mathbf{H}$.

Proof. See Lemma 12 in [1].

Now we are ready to prove the reliability of the error estimator.

Lemma 4.3. *Let* $\boldsymbol{\phi}$ *be the solution of* (15)*. If* (21) *and* (22) *hold, then*

$$\|\boldsymbol{\phi}\|_a \leq C \left\{ \eta_H + \left[\sum_{K \in \mathcal{T}_h} \frac{h_K^4}{\nu^3} \Big\{ \big(\|\boldsymbol{R}_K\|_{0,K} + \|\boldsymbol{f}\|_{0,K} \big) \|\boldsymbol{u}_h\|_{\infty,K} + \|\nabla\cdot \boldsymbol{u}_h\|_{0,K} \Big\}^2 \right]^{1/2} \right\}.$$

Proof. Using, Lemma 4.2 with $\boldsymbol{v} = \boldsymbol{\phi} - \mathcal{I}_h\boldsymbol{\phi}$, the mesh regularity, Cauchy–Schwarz inequality, (6) and (7),

it holds

$$\begin{aligned}\mathcal{R}_h^1(\boldsymbol{\phi}-\mathcal{I}_h\boldsymbol{\phi}) &\le C\nu^{1/2}\sum_{K\in\mathcal{T}_h} h_K^{-1}\,a(P_K\boldsymbol{\phi},P_K\boldsymbol{\phi})^{1/2}\|\boldsymbol{\phi}-\mathcal{I}_h\boldsymbol{\phi}\|_{0,K}\\ &\quad + C\nu^{1/2}\sum_{F\in\mathcal{E}_\Omega} h_F^{-1/2}\left[a(P_F\boldsymbol{\phi},P_F\boldsymbol{\phi})^{1/2}+\sum_{K'\subset\omega_F} a(P_{K'}\boldsymbol{\phi},P_{K'}\boldsymbol{\phi})^{1/2}\right]\|\boldsymbol{\phi}-\mathcal{I}_h\boldsymbol{\phi}\|_{0,F}\\ &\le C\left\{\sum_{K\in\mathcal{T}_h} a(P_K\boldsymbol{\phi},P_K\boldsymbol{\phi})+\sum_{F\in\mathcal{E}_\Omega} a(P_F\boldsymbol{\phi},P_F\boldsymbol{\phi})\right\}^{1/2}\\ &\quad\times\left\{\sum_{K\in\mathcal{T}_h}\nu h_K^{-2}\|\boldsymbol{\phi}-\mathcal{I}_h\boldsymbol{\phi}\|_{0,K}^2+\sum_{F\in\mathcal{E}_\Omega}\nu h_F^{-1}\|\boldsymbol{\phi}-\mathcal{I}_h\boldsymbol{\phi}\|_{0,F}^2\right\}^{1/2}\\ &\le C\,\eta_H\left\{\sum_{K\in\mathcal{T}_h}\|\boldsymbol{\phi}\|_{a,\tilde{\omega}_K}^2+\sum_{F\in\mathcal{E}_\Omega}\|\boldsymbol{\phi}\|_{a,\tilde{\omega}_F}^2\right\}^{1/2}\le C\,\eta_H\|\boldsymbol{\phi}\|_a. \end{aligned}\tag{23}$$

Now, from (15), Lemma 4.1, estimates (23) and (8), Cauchy–Schwarz inequality and mesh regularity, it holds

$$\begin{aligned}\|\boldsymbol{\phi}\|_a^2 &= a(\boldsymbol{\phi},\boldsymbol{\phi})=\mathcal{R}_h^1(\boldsymbol{\phi})=\mathcal{R}_h^1(\boldsymbol{\phi}-\mathcal{I}_h\boldsymbol{\phi})+\mathcal{R}_h^1(\mathcal{I}_h\boldsymbol{\phi})\\ &\le C\,\eta_H\|\boldsymbol{\phi}\|_a + C\nu^{-3/2}\sum_{K\in\mathcal{T}_h} h_K^2\Big\{(\|\boldsymbol{R}_K\|_{0,K}+\|\boldsymbol{f}\|_{0,K})\|\boldsymbol{u}_h\|_{\infty,K}+\|\nabla\cdot\boldsymbol{u}_h\|_{0,K}\Big\}\|\mathcal{I}_h\boldsymbol{\phi}\|_a\\ &\le C\left\{\eta_H^2+\sum_{K\in\mathcal{T}_h}\frac{h_K^4}{\nu^3}\Big[(\|\boldsymbol{R}_K\|_{0,K}+\|\boldsymbol{f}\|_{0,K})\|\boldsymbol{u}_h\|_{\infty,K}+\|\nabla\cdot\boldsymbol{u}_h\|_{0,K}\Big]^2\right\}^{1/2}\|\boldsymbol{\phi}\|_a,\end{aligned}$$

and the result follows.

From the previous results, we can state the following auxiliary equivalence theorem.

Theorem 4.2. *Let $\boldsymbol{\phi}$ be the solution of* (15)*, and assume that* (21) *and* (22) *hold. Then, there exist $C_1, C_2 > 0$, independents of h and ν, such that*

$$C_1\,\eta_H \le \|\boldsymbol{\phi}\|_a \le C_2\left\{\eta_H+\left[\sum_{K\in\mathcal{T}_h}\frac{h_K^4}{\nu^3}\Big\{\big(\|\boldsymbol{R}_K\|_{0,K}+\|\boldsymbol{f}\|_{0,K}\big)\|\boldsymbol{u}_h\|_{\infty,K}+\|\nabla\cdot\boldsymbol{u}_h\|_{0,K}\Big\}^2\right]^{1/2}\right\},$$

where η_H is given by (19).

Proof. The upper bound has been stated in Lemma 4.3. To proof the lower bound we first write the subspace $\mathbf{W}_h$ in the following way

$$\mathbf{W}_h=\mathbf{H}_h+\sum_{K\in\mathcal{T}_h}\mathbf{H}_K^b+\sum_{F\in\mathcal{E}_\Omega}\mathbf{H}_F^b=:\mathbf{H}_h+\sum_{i\in\mathcal{T}_h\cup\mathcal{E}_\Omega}\mathbf{H}_i^b.$$

From the definition of $P_i\boldsymbol{\phi}$ in (20), and by Cauchy–Schwarz's inequality we have

$$\begin{aligned}&\left[\sum_{i\in\mathcal{T}_h\cup\mathcal{E}_\Omega} a(P_i\boldsymbol{\phi},P_i\boldsymbol{\phi})\right]^2=\left[\sum_{i\in\mathcal{T}_h\cup\mathcal{E}_\Omega} a(\boldsymbol{\phi},P_i\boldsymbol{\phi})\right]^2=\left[a\left(\boldsymbol{\phi},\sum_{i\in\mathcal{T}_h\cup\mathcal{E}_\Omega}P_i\boldsymbol{\phi}\right)\right]^2\\ &\le a(\boldsymbol{\phi},\boldsymbol{\phi})\,a\left(\sum_{i\in\mathcal{T}_h\cup\mathcal{E}_\Omega}P_i\boldsymbol{\phi},\sum_{i\in\mathcal{T}_h\cup\mathcal{E}_\Omega}P_i\boldsymbol{\phi}\right)=a(\boldsymbol{\phi},\boldsymbol{\phi})\sum_{i\in\mathcal{T}_h\cup\mathcal{E}_\Omega}\sum_{j\in I_i}a(P_i\boldsymbol{\phi},P_j\boldsymbol{\phi})\\ &\le a(\boldsymbol{\phi},\boldsymbol{\phi})\sum_{i\in\mathcal{T}_h\cup\mathcal{E}_\Omega}\sum_{j\in I_i}\left\{\frac{1}{2}a(P_i\boldsymbol{\phi},P_i\boldsymbol{\phi})+\frac{1}{2}a(P_j\boldsymbol{\phi},P_j\boldsymbol{\phi})\right\}\le K_{\max}\,a(\boldsymbol{\phi},\boldsymbol{\phi})\sum_{i\in\mathcal{T}_h\cup\mathcal{E}_\Omega}a(P_i\boldsymbol{\phi},P_i\boldsymbol{\phi}),\end{aligned}\tag{24}$$

here I_i denotes the set of spaces $\mathbf{H}_j^b$ which are neighbors of $\mathbf{H}_i^b$, i.e.,

$$I_i := \{j : \exists \boldsymbol{v}_j \in \mathbf{H}_j^b \text{ and } \boldsymbol{v}_i \in \mathbf{H}_i^b \text{ such that } a(\boldsymbol{v}_i, \boldsymbol{v}_j) \neq 0\}$$

and $K_{\max}$ is the maximum number of neighbors, i.e.,

$$K_{\max} := \max\{\text{card}(I_l) : l \in \mathcal{T}_h \cup \mathcal{E}_\Omega\},$$

which is uniformly bounded due to the mesh regularity. Then, the result follows from (24), the definition of the norm $\|\cdot\|_a$ and noticing that

$$\eta_H^2 = \sum_{K\in\mathcal{T}_h} a(P_K\boldsymbol{\phi}, P_K\boldsymbol{\phi}) + \sum_{F\in\mathcal{E}_\Omega} a(P_F\boldsymbol{\phi}, P_F\boldsymbol{\phi}) = \sum_{i\in\mathcal{T}_h\cup\mathcal{E}_\Omega} a(P_i\boldsymbol{\phi}, P_i\boldsymbol{\phi}).$$

Finally, we establish the main result of this work. From (17), (19) and Theorem 4.2 the approximation error can be estimated as follows.

Theorem 4.3. *Let $(\boldsymbol{u}, p)$ and $(\boldsymbol{u}_h, p_h)$ be the solution of (1) and LPS, respectively, and suppose that (21) and (22) hold. Then*

$$C_1\tilde{\eta}_H \leq \|(\boldsymbol{u}-\boldsymbol{u}_h, p-p_h)\| \leq C_2\left(\tilde{\eta}_H + \left[\sum_{K\in\mathcal{T}_h}\frac{h_K^4}{\nu^3}\Big\{\big(\|\boldsymbol{R}_K\|_{0,K} + \|\boldsymbol{f}\|_{0,K}\big)\|\boldsymbol{u}_h\|_{\infty,K} + \|\nabla\cdot\boldsymbol{u}_h\|_{0,K}\Big\}^2\right]^{1/2}\right)$$

where

$$\tilde{\eta}_H^2 := \sum_{K\in\mathcal{T}_h}\tilde{\eta}_{H,K}^2$$

with

$$\tilde{\eta}_{H,K}^2 := \|P_K\boldsymbol{\phi}\|_{a,K}^2 + \frac{1}{2}\sum_{F\in\mathcal{E}(K)\cap\mathcal{E}_\Omega}\|P_F\boldsymbol{\phi}\|_{a,F}^2 + \nu\,\|\nabla\cdot\boldsymbol{u}_h\|_{0,K}^2,$$

and the positive constants C_1 and C_2 are independent of h.

Remark 4.5. *Note that the term*

$$T := \left(\sum_{K\in\mathcal{T}_h}\frac{h_K^4}{\nu^3}\Big\{(\|\boldsymbol{R}_K\|_{0,K} + \|\boldsymbol{f}\|_{0,K})\|\boldsymbol{u}_h\|_{\infty,K} + \|\nabla\cdot\boldsymbol{u}_h\|_{0,K}\Big\}^2\right)^{1/2},$$

appearing in Theorem 4.3, is, asymptotically, a high order term compared to $\tilde{\eta}_H$. In fact, we can see this, for instance, in Figures 1– 4 where we observe that $\tilde{\eta}_H$ is $\mathcal{O}(h)$ and T is $\mathcal{O}(h^2)$. For this reason we may omit T in our numerical tests. The behavior of this h.o.t. term is quite similar to $\left(\sum_{K\in\mathcal{T}_h} h_K^2\|\boldsymbol{f} - P_h\boldsymbol{f}\|_{0,K}^2\right)^{1/2}$, with $P_h\boldsymbol{f}$ a projection of $\boldsymbol{f}$, which appears in the a posteriori error estimates of the residual type (see Remark 1.8 in [31]).

5. Numerical validation

In order to validate our a posteriori error estimator we present some numerical tests. In examples 5.1 and 5.2 we analyze two problems with analytical solution in two and three dimensions, respectively, comparing in each case the exact approximation error with its estimated error $\tilde{\eta}_H$.

Also, as a mesure of the quality of our error estimator, we define the so called *effectivity index*, by

$$E_i := \frac{\tilde{\eta}_H}{\|(\boldsymbol{u}-\boldsymbol{u}_h, p-p_h)\|},$$

we expect that E_i remain bounded as h goes to 0 through a sequence of uniform refined meshes.

Finally, in examples 5.3 and 5.4, we address numerical comparisons with some well-documented benchmarks from the literature, namely, 2D driven cavity flow and 3D flow around a cylinder.

The adaptive procedure handles the nonlinearity by a Newton algorithm and uses a structured coarse mesh to start the process. At each step, we solve the LPS problem and compute its corresponding local error estimator $\tilde{\eta}_{H,K}$ for each element $K \in \mathcal{T}_h$, and refine those elements accordingly to

$$\tilde{\eta}_{H,K} \geq \theta \max\{\tilde{\eta}_{H,K'} : K' \in \mathcal{T}_h\},$$

where $\theta \in]0,1[$ is a prescribed parameter. Then we evaluate the stopping criterion and decide to finish or go to the next step. In addition, when it comes to adapt meshes, the solution computed in the previous mesh, after an interpolation process on the current mesh [25], is set as the initial guess solution for the Newton iteration method in the current mesh.

In the case $\nu \ll 1$, the numerical algorithm demands a continuation strategy to reach the target viscosity. This strategy consists in beginning with a relatively big viscosity value and decreasing it gradually to attain the desired value.

For practical purposes, we used the mesh generators `Triangle` [27] and `Tetgen` [28] to create the initial and adapted meshes in 2D and 3D, respectively, as it allowed us to create successively refined meshes based on a hybrid Delaunay refinement algorithm.

Remark 5.1. *Note that problem (NS) have homogeneous Dirichlet boundary condition, but in our numerical examples we consider both non homogeneous Dirichlet and Neumann boundary conditions, which are not covered by our theory. The changes necessary to deal with these boundary conditions are: in the case of non homogeneous Dirichlet conditions it appears an extra term in the estimator that measures the error in the approximation of the exact Dirichlet condition, in general, this is a high order term that can be neglected in the numerical computations. In the case of Neumann boundary conditions it is necessary to change the rhs of the equation and add, to the definition of $\tilde{\eta}_H$ in* (19)*, the terms $a(P_F\boldsymbol{\phi}, P_F\boldsymbol{\phi})$ for the edges F on the Neumann boundary.*

5.1. Two-dimensional analytic solution

In this example we consider $\Omega =]0,1[^2$ and the boundary conditions such as the exact solution is given by $\boldsymbol{u}(x,y) := (u_1(x,y), u_2(x,y))$, with

$$u_1(x,y) := 256\, y^2(y-1)^2 x(x-1)(2x-1),$$
$$u_2(x,y) := -u_1(y,x),$$

and

$$p(x,y) := 150(x-0.5)(y-0.5).$$

For the viscosity we consider the cases: $\nu = 1, 10^{-2}$.

The error, a posteriori estimator and effectivity index are shown in Tables 1 and 2 for $\nu = 1$ and $\nu = 10^{-2}$, respectively. Likewise, the corresponding convergence history for $\nu = 1$ and $\nu = 10^{-2}$ is presented in Figures 1 and 2.

Table 1: Exact error, a posteriori error estimator and effectivity index for the 2D example with analytical solution with $\nu = 1$.

h	$\|(u-u_h, p-p_h)\|$	$\tilde{\eta}_H$	E_i
0.031250	0.557676	0.523659	0.939002
0.015625	0.276208	0.263430	0.953736
0.007813	0.137523	0.132090	0.960493
0.003906	0.068629	0.066137	0.963677
0.001953	0.034284	0.033091	0.965216

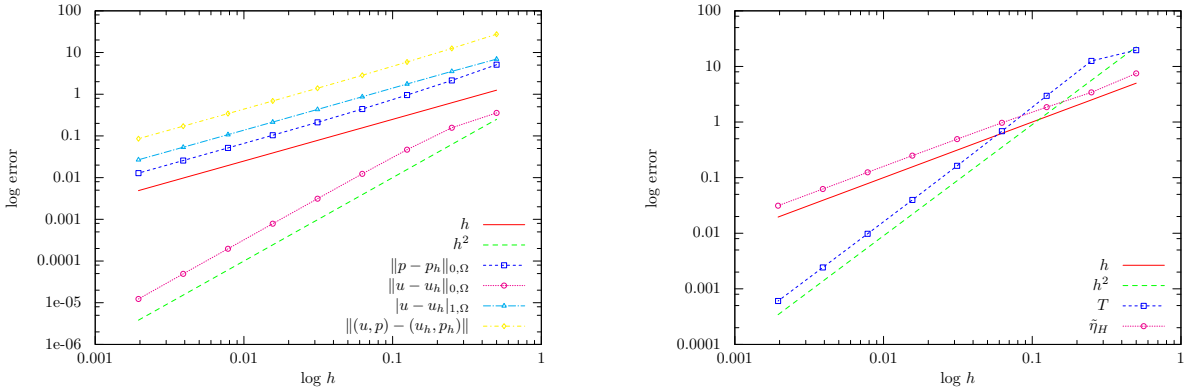

Figure 1: Convergence history for the 2D example with analytical solution, case $\nu = 1$ (left) and the behavior of T when h goes to 0 (right).

Table 2: Exact error, a posteriori error estimator and effectivity index for the 2D example with analytical solution with $\nu = 10^{-2}$.

h	$\|\|(u - u_h, p - p_h)\|\|$	$\tilde{\eta}_H$	E_i
0.031250	3.656915	2.163265	0.591555
0.015625	1.684914	1.075223	0.638147
0.007813	0.811511	0.533646	0.657596
0.003906	0.400764	0.266174	0.664166
0.001953	0.199667	0.132940	0.665810

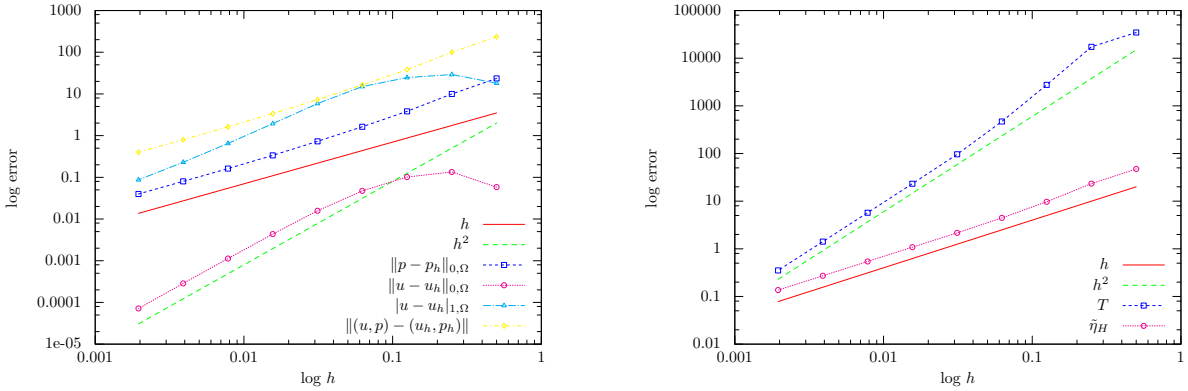

Figure 2: Convergence history for the 2D example with analytical solution, case $\nu = 10^{-2}$ (left) and the behavior of T when h goes to 0 (right).

In both cases, $\nu = 1$ or $\nu = 10^{-2}$, we observe a good agreement between the numerical results and the results predicted by the theory.

5.2. Three-dimensional analytic solution

We consider $\Omega :=]0, 1[^3$ and choose the data $\boldsymbol{f}$ so that the exact solution is given by

$$\boldsymbol{u}(x, y, z) := (e^x \sin(z),\ -e^x \sin(z),\ e^x \cos(z) - e^x \cos(y))$$

and

$$p(x,y) := \frac{-1}{2}e^{2x} + \frac{1}{4}(e^2 - 1).$$

As in the 2D example, we analyze the cases $\nu = 1,\ 10^{-2}$.

In Figures 3 and 4, we summarize the convergence history of the LPS method with $\nu = 1$ and $\nu = 10^{-2}$, respectively. Also, in Tables 3 and 4 we show the exact error, a posteriori error estimator and effectivity index for the cases $\nu = 1$ and $\nu = 10^{-2}$.

Table 3: Exact error, a posteriori error estimator and effectivity index for the 3D example with analytical solution with $\nu = 1$.

h	$\|(\boldsymbol{u} - \boldsymbol{u}_h, p - p_h)\|$	$\tilde{\eta}_H$	E_i
0.444081	0.544975	0.438047	0.803793
0.247472	0.283073	0.232354	0.820826
0.143330	0.150263	0.131043	0.872088
0.081658	0.080683	0.072337	0.896558
0.045780	0.043711	0.039629	0.906613

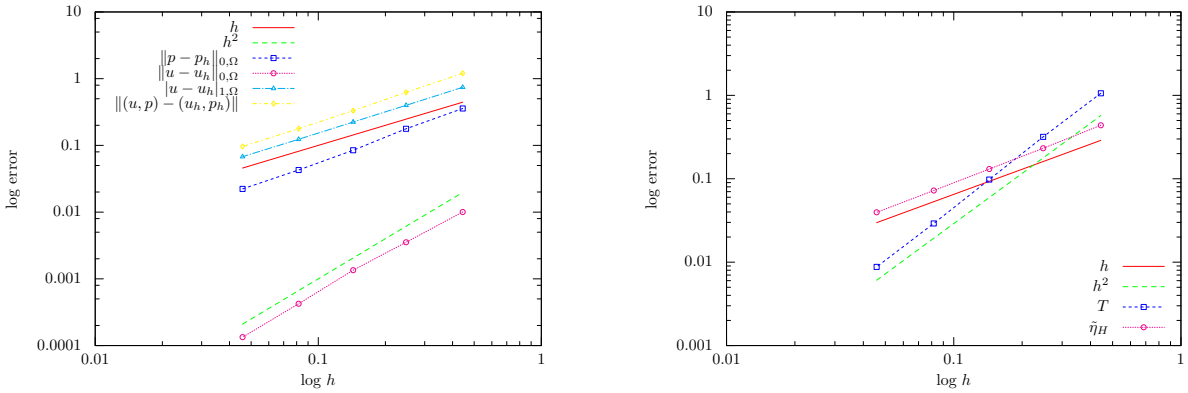

Figure 3: Convergence history for the 3D example with analytical solution, case $\nu = 1$ (left) and the behavior of T when h goes to 0 (right).

Table 4: Exact error, a posteriori error estimator and effectivity index for the 3D example with analytical solution with $\nu = 10^{-2}$.

h	$\|(\boldsymbol{u} - \boldsymbol{u}_h, p - p_h)\|$	$\tilde{\eta}_H$	E_i
0.2474718	2.8269643	0.4619786	0.1634186
0.1433296	1.2279783	0.2728947	0.2222309
0.0816576	0.5090968	0.1525166	0.2995827
0.0457801	0.2144706	0.0848238	0.3955032

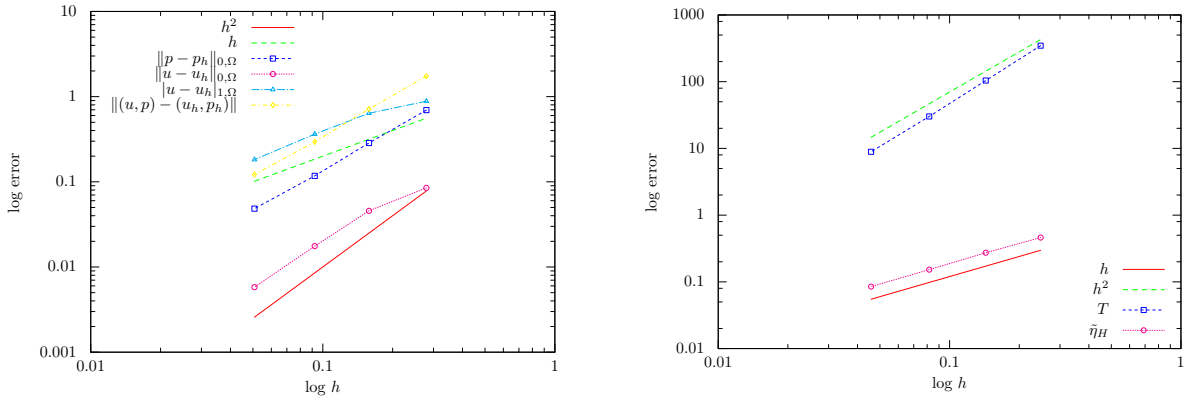

Figure 4: Convergence history for the 3D example with analytical solution, case $\nu = 10^{-2}$ (left) and the behavior of T when h goes to 0 (right).

Remark 5.2. *Note that from Tables 1–2 and Tables 3–4 we observe that the errors grow when we change ν from 1 to 10^{-2}, which means that we have some inrobustness with respect to ν. In our computations for the Stokes problem we observe the same phenomena, this lead us to think that the problem is the lack of robustness of the method related to the pressure in the sense of [23].*

5.3. Two-dimensional lid-driven cavity problem

In this case we considered the well-known 2D cavity problem, where the domain Ω is $]0,1[\times]0,1[$, $\boldsymbol{f} = \mathbf{0}$ and the boundary conditions are defined as in Figure 5 (we refer the reader to [18], [24] and [29] for a complete bibliography on this problem). In our particular case, $\nu = 1/Re$, with Reynolds number $Re = 5,000$.

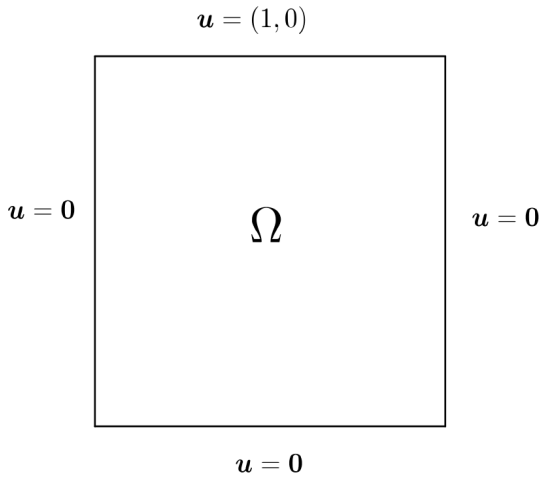

Figure 5: Domain and boundary conditions for the driven cavity problem.

The Figure 6 depicts the final mesh obtained with our adaptive scheme together the streamlines given by the solution obtained using that mesh. We observe that mesh refinement concentrates mainly around the primary vortex but also we recover secondary vortices in the expected locations.

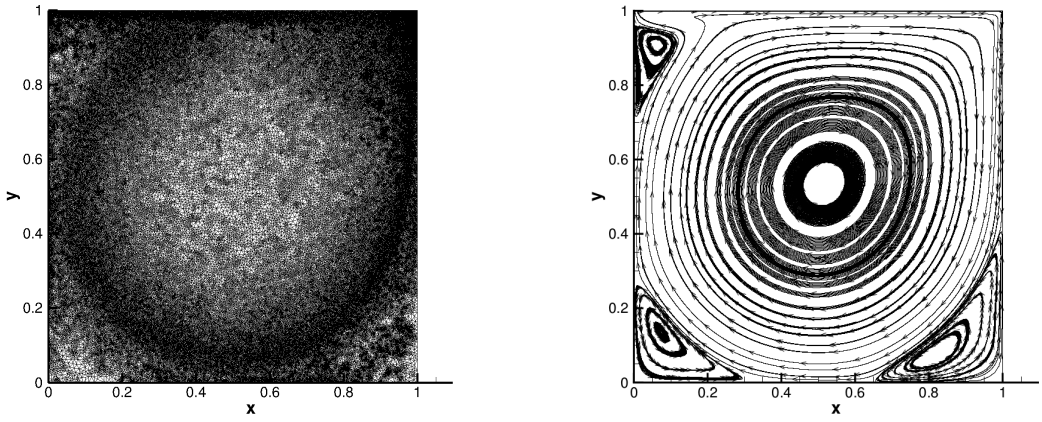

Figure 6: Lid-driven cavity problem for $Re = 5,000$. Adaptive mesh and streamlines. The mesh has 345,947 elements.

In Table 5, we compare our results with the ones obtained from other approaches in the literature. Note that we get similar values compared with others solvers.

Scheme	x	y
Ghia *et al.* (1982)	0.5117	0.5352
Medic & Mohammadi (1999)	0.53	0.53
LPS $\mathbb{P}_1 \times \mathbb{P}_0$	0.5156	0.5343

Table 5: Position of the center of the primary vortex. The LPS results were obtained with the adaptive mesh of Figure 6.

5.4. Flow around of a circular cylinder

This problem, depicted in Figure 7, represents a channel with a cylindrical obstacle. The domain Ω is the region $]0, 2.5[\times]0, H[\times]0, H[$, with $H = 0.41$m, without a cylinder of diameter $D = 0.1$ m. The inflow velocity field is

$$\boldsymbol{u}_p = H^{-4}\big(16Uyz(H-y)(H-z),\, 0,\, 0\big)^t,$$

with $U = 0.45$ m/s, the fluid viscosity is given by $\nu = 10^{-3}$ and the right-hand side of the momentum equation vanishes, i.e. $\boldsymbol{f} = \boldsymbol{0}$. For further details see [22] and [26].

The benchmark coefficients to compute are the following three: the pressure difference Δp between the points $(0.55, 0.2, 0.205)$ and $(0.45, 0.2, 0.205)$, and the *drag* and *lift* coefficients defined as follows:

$$C_{\text{drag}} := \frac{2F_{\text{drag}}}{\rho\bar{u}^2 DH} \quad \text{and} \quad C_{\text{lift}} := \frac{2F_{\text{lift}}}{\rho\bar{u}^2 DH},$$

where $\rho = 1$ and $\bar{u} = 0.2$, are the density of the fluid and the mean inflow, respectively, and

$$F_{\text{drag}} := \int_S \left(\rho\nu \frac{\partial u_t}{\partial \boldsymbol{n}} n_y - p\, n_x\right) \mathrm{d}S \quad \text{and} \quad F_{\text{lift}} := \int_S \left(\rho\nu \frac{\partial u_t}{\partial \boldsymbol{n}} n_x - p\, n_y\right) \mathrm{d}S$$

be the *drag* and *lift* forces, respectively. Here S is the surface of the cylinder, $\boldsymbol{n} = (n_x, n_y, n_z)$ the inward pointing unit vector with respect to Ω, $\boldsymbol{t}$ a tangential vector on S and $u_t = \boldsymbol{u} \cdot \boldsymbol{t}$ is the projection of the velocity into the direction $\boldsymbol{t}$.

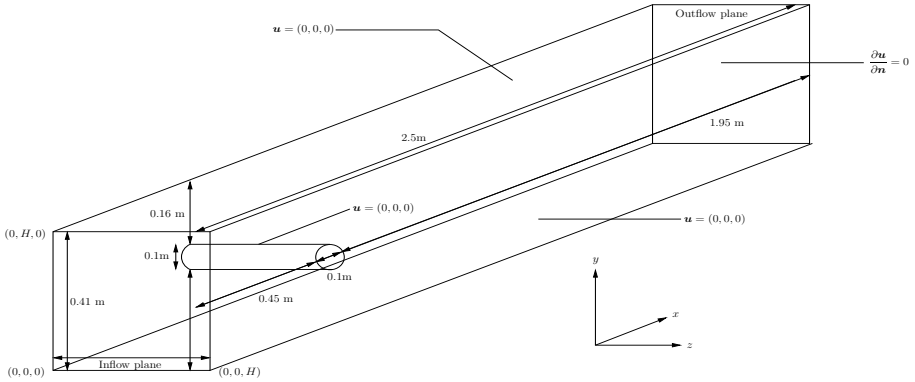

Figure 7: Configuration of the cylinder benchmark problem.

The Table 6 shows the results from the LPS method obtained from the adaptive meshes. The reference intervals for the three coefficients (see [22]) are: $C_{\text{drag}} \in [6.05, 6.25]$, $C_{\text{lift}} \in [0.008, 0.01]$ and $\Delta p \in [0.165, 0.175]$.

elements	C_{drag}	C_{lift}	Δp
628,725	6.1911	0.0173540	0.17092
908,760	6.1236	0.0078108	0.16566
1,080,148	6.1023	0.0082491	0.17000

Table 6: The benchmark coefficients C_{drag}, C_{lift} and Δp.

In Figure 8 we show the final adapted mesh, obtained with our adaptive scheme, and a zoom of a cut made at $z = 0.205$. Note, as expected, that most of the refinement is done near the cylinder. To complement the information, in Figure 9 we show the streamtracers of the velocity field and in Figure 10 the magnitude of the velocity and the pressure at the cross-section $z = 0.205$ in the final adapted mesh. Observe that the overall results are in accordance with the expected behavior of the flow (see, for instance, [5] and [9]).

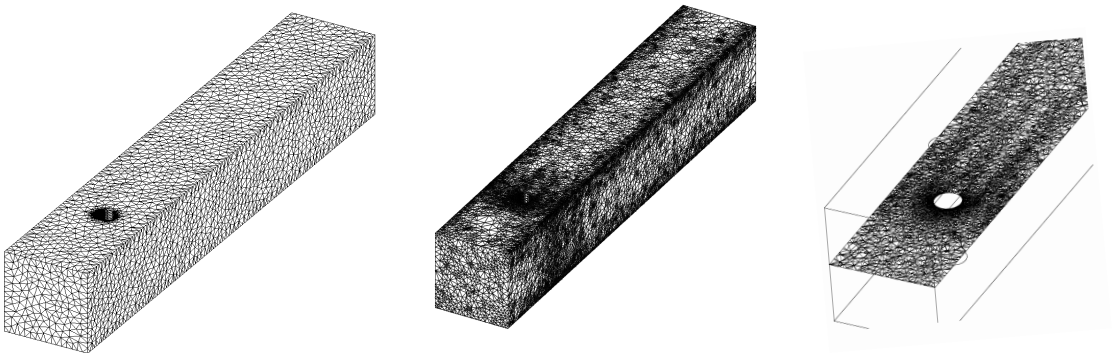

Figure 8: Initial mesh (left), final adapted mesh with 1,080,148 elements (center) and a cut through the plane $z = 0.205$ (right).

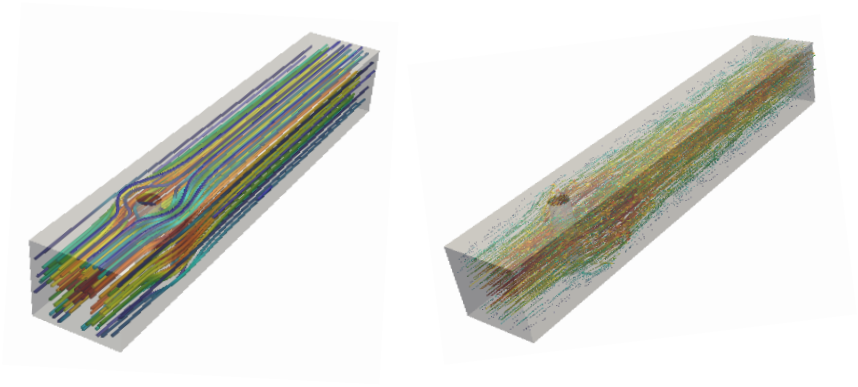

Figure 9: Sreamtracers (left) and velocity vector field (right).

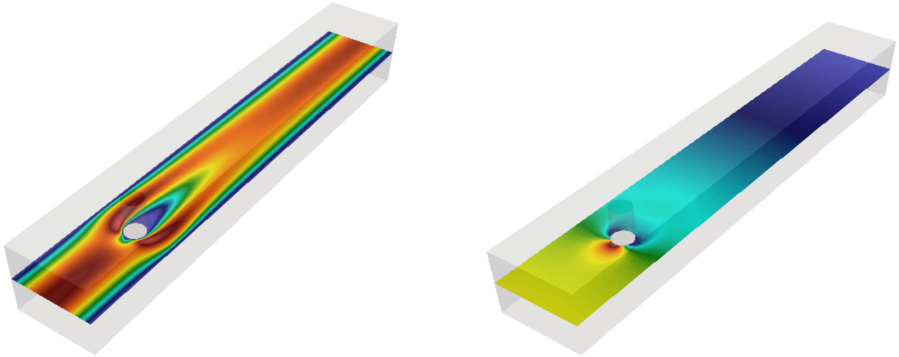

Figure 10: Isovalues of the magnitude of the velocity field (left) and of the pressure (right).

Remark 5.3. *A more accurate approximation of the drag and lift coefficients is presented in [13], where the authors used a $\mathbb{Q}_2$ approximation joint with an a posteriori error estimator based in the computation of quantities of interest. Note that our estimator is designed with an "energy norm" in mind, then it is not optimal in the sense of the computation of those parameters. On the other hand, a goal oriented estimator is, normally, more expensive to compute due to the cost implied in solving the dual problem.*

6. Conclusions

In this paper we adapted the ideas of [1] and [3] to develop an a posteriori error analysis of hierarchical-type for the LPS method, introduced in [5], which approximates the solution of the fully nonlinear incompressible Navier–Stokes equations. Our a posteriori estimator is based on the solution of local problems posed in specific one-dimensional spaces of bubble-like functions, so is easy to implement with low computational cost. In order to study the performance of our a posteriori estimator we presented numerical examples with analytical solutions checking that the effectivity index stays bounded as h goes to zero, and we tested well known benchmark problems which live outside of the theoretical framework showing that our a posteriori estimator generates a sequence of adapted meshes improving the quality of the numerical solutions even in turbulent regime, as was shown with the lid-driven cavity problem.

Acknowledgements

The first author was partially founded by CONICYT/Chile through FONDECYT project N° 1150174, Basal project CMM–CI2MA PFB–03 and Red Doctoral REDOC.CTA, MINEDUC project UCO1202 at

Universidad de Concepción. The second author was funded by CONICYT/Chile through Becas Chile program and Universidad de Concepción.

References

[1] Araya, R., Barrenechea, G. R., Poza, A., 2008. An adaptive stabilized finite element method for the generalized Stokes problem. J. Comput. Appl. Math. 214 (2), 457–479.
[2] Araya, R., Poza, A. H., Stephan, E. P., 2005. A hierarchical a posteriori error estimate for an advection-diffusion-reaction problem. Math. Models Methods Appl. Sci. 15 (7), 1119–1139.
[3] Araya, R., Poza, A. H., Valentin, F., 2012. On a hierarchical error estimator combined with a stabilized method for the Navier–Stokes equations. Numer. Methods Partial Differential Equations 28 (3), 782–806.
[4] Araya, R., Poza, A. H., Valentin, F., 2014. An adaptive Residual Local Projection finite element method for the Navier–Stokes equations. Adv. Comput. Math 40 (5-6), 1093–1119.
[5] Araya, R., Poza, A. H., Valentin, F., 2016. A low-order local projection method for the incompressible Navier–Stokes equations in two- and three-dimensions. IMA J. Numer. Anal. 36 (1), 267–295.
[6] Bank, R., Smith, K., 1993. A posteriori error estimates based on hierarchical bases. SIAM J. Numer. Anal. 30 (4), 921–935.
[7] Bank, R., Weiser, A., 1985. Some a posteriori error estimators for elliptical partial differential equations. Math. Comp. 44, 283–301.
[8] Barrenechea, G. R., Valentin, F., 2010. A residual local projection method for the Oseen equation. Comput. Methods Appl. Mech. Engrg. 199 (29–32), 1906–1921.
[9] Bayraktar, E., Mierka, O., Turek, S., 2012. Benchmark computations of 3D laminar flow around a cylinder with CFX, OpenFOAM and FeatFlow. Int. J. Comput. Sci. Eng. 7 (3), 253–266.
[10] Becker, R., Braack, M., 2001. A finite element pressure gradient stabilization for the Stokes equations based on local projections. Calcolo 38 (4), 173–199.
[11] Berrone, S., 2001. Adaptive discretization of stationary and incompressible Navier–Stokes equations by stabilized finite element methods. Comput. Methods Appl. Mech. Engrg. 190 (34), 4435–4455.
[12] Braack, M., Burmann, E., 2006. Local projection stabilization for the Oseen problem and its interpretation as a variational multiscale method. SIAM J. Numer. Anal. 43 (6), 2544–2566.
[13] Braack, M., Richter, T., 2006. Solutions of 3D Navier-Stokes benchmark problems with adaptive finite elements. Computers & Fluids 35 (4), 372–392.
[14] Brooks, A. N., Hughes, T. J. R., 1982. Streamline Upwind/Petrov-Galerkin formulations for convection dominated flows with particular emphasis on the incompressible Navier-Stokes equations. Comput. Methods Appl. Mech. Engrg. 32, 199–259.
[15] Clément, P., 1975. Approximation by finite element functions using local regularization. R.A.I.R.O. Anal. Numer. 9, 77–84.
[16] Ern, A., Guermond, J. L., 2004. Theory and Practice of Finite Elements. Vol. 159 of Applied Mathematical Sciences. Springer-Verlag, New York.
[17] Franca, L. P., Frey, S., 1992. Stabilized finite element methods. II. The incompressible Navier–Stokes equations. Comput. Methods Appl. Mech. Engrg. 99 (2–3), 209–233.
[18] Ghia, U., Ghia, K., Shin, C., 1982. High-Re solutions for incompressible flow using the Navier–Stokes equations and a multigrid method. J. Comput. Phys. 48 (3), 387–411.
[19] Girault, V., Raviart, P. A., 1986. Finite Element Methods for Navier–Stokes Equations: Theory and Algorithms. Vol. 5 of Springer Series in Computational Mathematics. Springer–Verlag, Berlin.
[20] Hughes, T. J., Franca, L. P., Balestra, M., 1986. A new finite element formulation for computational fluid dynamics: V. Circumventing the Babuska-Brezzi condition: A stable Petrov-Galerkin formulation of the Stokes problem accommodating equal-order interpolations. Comput. Methods Appl. Mech. Engrg. 59 (1), 85–99.
[21] John, V., 2001. Residual a posteriori error estimates for two-level finite element methods for the Navier–Stokes equations. Appl. Numer. Math. 37 (4), 503–518.
[22] John, V., 2002. Higher order finite element methods and multigrid solvers in a benchmark problem for the 3D Navier–Stokes equations. Int. J. Numer. Meth. Fluids 40 (6), 775–798.
[23] Linke, A., Merdon, C., 2016. Pressure-robustness and dicrete Helmholtz projectors in mixed finite element methods for the incompressible Navier-Stokes equations. Comput. Methods Appl. Mech. Engrg. 311, 304–326.
[24] Medic, G., Mohammadi, B., 1999. NSIKE – An incompressible Navier–Stokes solver for unstructured meshes. Tech. Rep. 3644, INRIA, Rocquencourt.
[25] Renka, R., 1988. Algorithm 660: QSHEP2D: Quadratic Shepard method for bivariate interpolation of scattered data. ACM Trans Math Softw 14., 149 – 150.
[26] Schäfer, M., Turek, S., Durst, F., Krause, E., Rannacher, R., 1996. Flow Simulation with High-Performance Computers II: DFG Priority Research Programme Results 1993–1995. Vieweg+Teubner Verlag, Wiesbade, Ch. Benchmark Computations of Laminar Flow Around a Cylinder, pp. 547–566.
[27] Shewchuk, J. R., 1996. Triangle: Engineering a 2D quality mesh generator and Delaunay triangulator. In: Applied computational geometry towards geometric engineering. Vol. 1148. Springer–Verlag, Berlin, pp. 203–222.
[28] Si, H., 2015. Tetgen, a Delaunay-based quality tetrahedral mesh generator. ACM Trans. Math. Softw. 41 (2), 11:1–11:36.
[29] Turek, S., 1999. Efficient Solvers for Incompressible Flow Problems. Vol. 6 of Lect. Notes Comput. Sci. Eng. Springer–Verlag, Berlin.

[30] Verfürth, R., 1994. A posteriori error estimates for nonlinear problems. finite element discretizations of elliptic equations. Math. Comp. 62 (206), 445–475.
[31] Verfürth, R., 2013. A Posteriori Error Estimation Techniques for Finite Element Methods. Numerical Mathematics and Scientific Computation. Oxford University Press, Oxford.

Centro de Investigación en Ingeniería Matemática (CI^{2}MA)

PRE-PUBLICACIONES 2017 - 2018

2017-22 Rolando Biscay, Joaquin Fernández, Carlos M. Mora: *Numerical solution of stochastic master equations using stochastic interacting wave functions*

2017-23 Gabriel N. Gatica, Mauricio Munar, Filander A. Sequeira: *A mixed virtual element method for the Navier-Stokes equations*

2017-24 Nicolas Barnafi, Gabriel N. Gatica, Daniel E. Hurtado: *Primal and mixed finite element methods for deformable image registration problems*

2017-25 Sergio Caucao, Gabriel N. Gatica, Ricardo Oyarzúa: *A posteriori error analysis of an augmented fully-mixed formulation for the non-isothermal Oldroyd-Stokes problem*

2017-26 Raimund Bürger, Stefan Diehl, María Carmen Martí: *A conservation law with multiply discontinuous flux modelling a flotation column*

2017-27 Antonio Baeza, Raimund Bürger, Pep Mulet, David Zorío: *Central WENO schemes through a global average weight*

2017-28 Rodolfo Araya, Manuel Solano, Patrick Vega: *Analysis of an adaptive HDG method for the Brinkman problem*

2017-29 Sergio Caucao, Marco Discacciati, Gabriel N. Gatica, Ricardo Oyarzúa: *A conforming mixed finite element method for the Navier-Stokes/Darcy-Forchheimer coupled problem*

2017-30 Tonatiuh Sanchez-Vizuet, Manuel Solano: *A Hybridizable Discontinuous Galerkin solver for the Grad-Shafranov equation*

2017-31 David Mora, Gonzalo Rivera: *A priori and a posteriori error estimates for a virtual element spectral analysis for the elasticity equations*

2017-32 Gabriel N. Gatica, Mauricio Munar, Filander A. Sequeira: *A mixed virtual element method for a nonlinear Brinkman model of porous media flow*

2018-01 Rodolfo Araya, Ramiro Rebolledo: *An a posteriori error estimator for a LPS method for Navier-Stokes equations*

Para obtener copias de las Pre-Publicaciones, escribir o llamar a: Director, Centro de Investigación en Ingeniería Matemática, Universidad de Concepción, Casilla 160-C, Concepción, Chile, Tel.: 41-2661324, o bien, visitar la página web del centro: http://www.ci2ma.udec.cl







Centro de Investigación en
Ingeniería Matemática (CI²MA)
Universidad de Concepción

Casilla 160-C, Concepción, Chile
Tel.: 56-41-2661324/2661554/2661316
http://www.ci2ma.udec.cl